Twist-bend nematic drops as colloidal particles: Structural features

K. S. Krishnamurthy,* D. S. Shankar Rao, Santosh Y. Khatavi, and Channabasaveshwar V. Yelamaggad
Centre for Nano and Soft Matter Sciences, Survey No. 7, Shivanapura, Bangalore 562162, India

(Received 9 January 2023; accepted 14 March 2023; published 28 March 2023)

The mesogen CB7CB [1″,7″-bis(4-cyanobiphenyl-4′-yl)heptane], mixed with a small quantity of a long chain amphiphile, is examined for the structural features of twist-bend nematic (N_{TB}) drops acting as colloidal inclusions in the isotropic and nematic environments. In the isotropic phase, the drops nucleating in the radial (splay) geometry develop toward escaped radial, off-centered structures, involving both splay and bend distortions. With further growth, they transform into low-birefringence (near-homeotropic) objects, within which remarkably well-organized networks of parabolic focal conic defects evolve in time. In electrically reoriented near-homeotropic N_{TB} drops, the pseudolayers develop an undulatory boundary possibly attributable to saddle-splay elasticity. In the matrix of the planar nematic phase, N_{TB} droplets appearing as radial hedgehogs attain stability in the dipolar geometry, through their association with hyperbolic hedgehogs. With growth, on transformation of the hyperbolic defect into its topologically equivalent Saturn ring around the N_{TB} drop, the geometry turns quadrupolar. Significantly, dipoles are stable in smaller drops, while quadrupoles are stable in larger ones. The dipole-quadrupole transformation is reversible, but is hysteretic with respect to drop size. Importantly, this transformation is often mediated by nucleation of two loop disclinations, one appearing at a marginally lower temperature than the other. The existence of a metastable state with partial formation of a Saturn ring and persistence of the hyperbolic hedgehog raises a question relating to the conservation of topological charge. In twisted nematics, this state features in the formation of a giant unknot that binds all N_{TB} drops together.

DOI: 10.1103/PhysRevE.107.034706

I. INTRODUCTION

The twist-bend or heliconical nematic phase (N_{TB}) is made of achiral, flexible-core bent molecules that wind obliquely around an axis (twist vector $\boldsymbol{\chi}$), clockwise or anticlockwise with equal probability. The N_{TB} structure, with its unique nanometric helical pitch, is promoted in nematogens of very low bend elastic modulus k_{33}, such as the well-known dimer CB7CB [1,2]. Belonging to the D_∞ point group, with a local C_2 axis of symmetry, it is considered structurally intermediate between the ordinary nematic (N) phase (point group $D_{\infty h}$) of achiral molecules orientationally ordered along a preferred direction (the director, **n**), and the cholesteric (N^*) phase (point group D_∞) of chiral molecules organized with their C_∞ axis precessing orthogonally about a common axis [3]. An important feature of the N_{TB} helix is its association with a correspondingly winding local polarization vector **P** directed transversely to $\boldsymbol{\chi}$ and **n** (local) [4]. This N_{TB} phase, visualized early by Meyer [5] in the context of the flexoelectric phenomenon, has been under intense study for over a decade now because of its many challenging properties of fundamental significance. For example, despite the x-ray evidence of the absence of periodic mass density variations in it [1], the N_{TB} phase behaves as a pseudolayered phase. When derived from a planar nematic N, even in the absence of any external field, it exhibits a striped state, with a micrometric modulation directly related to sample thickness; this is believed to be due to a Helfrich-Hurault-type mechanism causing the pseudolayers of thickness equal to the helical pitch to undergo three-dimensional (3D) undulations [6]. The smecticlike behavior of the N_{TB} phase is also evident in the thermodynamically stable parabolic focal conic defects (PFCDs) that it often develops [7–9]. The stability of these PFCDs, over elliptohyperbolic and toric FCDs, has been interpreted using the extended Volterra process, in terms of the presence or absence of defect densities attached to the conics [10].

In most studies on the N_{TB} phase, the sample used is a laterally unrestricted thin monophasic layer. Recently, it has been found that droplets of this phase dispersed in the matrix of the precursor nematic phase constitute an interesting colloidal system with which to generate diverse topological entities like dipoles, quadrupoles, and their chained and knotted assemblies [11]. Such a system, besides its obvious advantage over conventional nematic colloids made of solid or fluid particle dispersions in controlling the droplet size by means of temperature, also enables a study of structural changes taking place within the dispersed drops in different biphasic regimes. The latter aspect is demonstrated in the radically new growth behavior of N_{TB} drops embedded in the nematic matrix; the drops, initially in the Frank-Pryce (FP) geometry, like the Robinson cholesteric spherulites [12], develop fingerlike outgrowths with new disclinations not belonging to the FP structure and emanating from the homeotropic region that replaces the +1 point defect. In the model used to understand these effects, the +1 point defect is visualized as expanding into polygonal loops. Contrastingly, the point

*murthyksk@gmail.com

 ©2023 American Physical Society

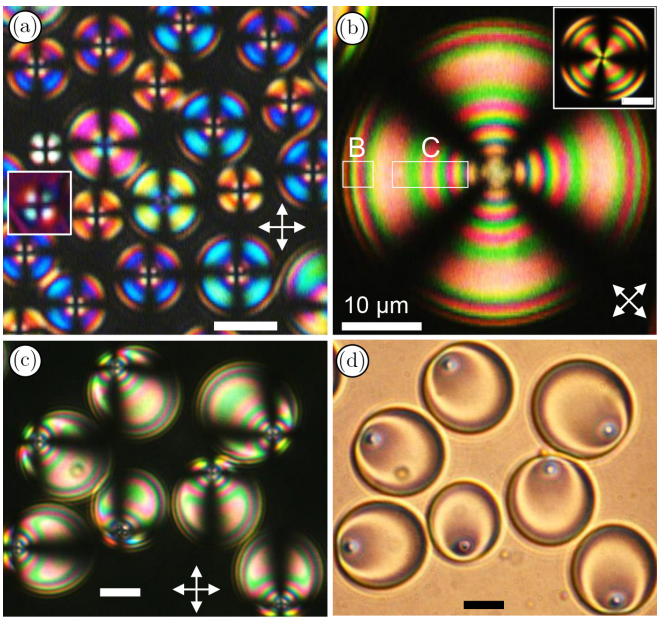

FIG. 1. (a,b) Radial N_{TB} drops in isotropic matrix; 20 μm thick layer of *C*-OP5 in a planar cell; $T = 88$ °C (a), 89.4 °C (b). The drop in (b) is under a sine wave field ($U = 15$ V, $f = 10$ kHz) inducing discernible realignment in the core region, but not in the outer region. Inset to (a) shows the low-birefringence drop above it, but with a full-wave plate; the increase in color is along the diagonal corresponding to the slow axis of the retarder. Inset to (b) shows a toroidal N_{TB} drop in a homeotropically aligned layer of *C*-TA5 (see [11]). (c,d) Point defects of the radial hedgehogs become off centered as the drops grow, with their χ field tending toward the escaped radial geometry.

defect of the Robinson spherulite does not change into a loop as it is of no energetic advantage in cholesterics since the χ field there, unlike in the N_{TB}, is not materialized [11]. Other recent studies, again using CB7CB-surfactant mixtures, have shown (a) varied electrokinetic effects of flexodielectric origin in topological dipoles [13], (b) several morphological and electrokinetic features of dispersed *nematic* drops [14], and (c) thermomechanical (Lehmann) rotation of twisted bipolar *nematic* droplets suspended in the isotropic liquid [15]. Continuing this line of investigation, we have now studied various structural and electrokinetic aspects of N_{TB} drops acting as colloidal inclusions in both nematic and isotropic environments. The main findings of this study are (a) progressive transformation of the radial hedgehog geometry of N_{TB} drops into a network of PFCDs, (b) existence of a metastable topological state of a "fractional" Saturn ring linked to the hyperbolic hedgehog, (c) dipole-quadrupole transition mediated by nucleation of additional loop defects, (d) formation of a giant unknot in twist cells through three types of disclination link, (e) flexodielectric responses of PFCDs, and (f) electric propulsion of escaped radial drops. In this paper, we present the results (a)–(d) relating to the structural aspects; electrically induced phenomena in colloidal N_{TB} drops, (e) and (f), will be reported separately. Our presentation of the results in Sec. III is supplemented by nine movie clips, some optical microscopic textures, and connected notes, which are accessible in the Supplemental Material (SM) [16].

II. EXPERIMENTS

The compound CB7CB used in this study was synthesized by two of the authors (S.Y.K. and C.V.Y.). As determined by polarization microscopy, it had the following phase sequence: N_{TB}(103.3 °C) *N* (116.5 °C) *I*. N_{TB} drops were studied in the N_{TB}-*N* and N_{TB}-*I* coexistence regions using binary mixtures of CB7CB with an amphiphilic dopant. The mixtures are referred to as *C*-OP*i* and *C*-TA*i*, where C, OP, TA, and *i* denote, respectively, CB7CB, 2-octadecoxypropanol, 1-tetradecanoic acid, and concentration of the dopant in wt %. With *i* in the range 3–8, coexisting biphasic regions of a few °C range could be obtained; with higher *i*, the surfactant-rich phase showed a tendency to separate as droplets. The phase diagram of *C*-TA in Fig. S1 of the SM in Ref. [11] is typical of the transitional behavior of the mixtures. In the most commonly used mixtures, the *I*-*N* and *N*-N_{TB} onset temperatures T_N and T_{NTB} were $T_N = 102.5$ °C (*C*-OP3), 99.0 °C (*C*-OP5), 94.7 °C (*C*-OP7), and 102.5 °C (*C*-TA5), and $T_{NTB} = 91.0$ °C (*C*-OP3), 90.0 °C (*C*-OP5), 89.2 °C (*C*-OP7), and 93.5 °C (*C*-TA5). On a prolonged use of the mixtures, particularly in high electric fields, we noticed a slight degradation of the sample leading to a decrease in the transition temperatures by 1 °C–2 °C; but this did not affect the morphological features of the drops investigated. The dielectric anisotropy

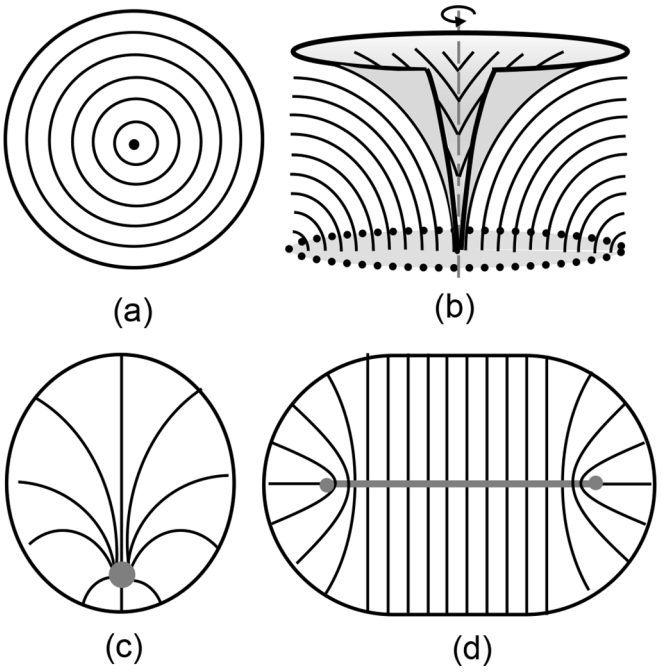

FIG. 2. Schematic of pseudolayers of the heliconical phase in N_{TB} drops. (a) A small drop of planform diameter $D < d$ with the radial hedgehog configuration, in the isotropic matrix. (b) Toroidal focal conic structure with singularities along the rotational axis (vertical dashed line along the layer normal) and the circle (dotted line) attached to the bottom substrate; pseudolayers with the twist director transverse to them are indicated by parallel equidistant curves. (c) Off-centered ellipsoidal drop with a splay-bend distortion field. (d) Oblate spheroidal drop with central homeotropic alignment and a circular $+\frac{1}{2}$ disclination loop (in gray) in place of the +1 point defect. Director field is indicated by thin lines.

($\varepsilon_a = \varepsilon_{||} - \varepsilon_{\perp}$) for the pure CB7CB sample used in the mixtures was positive, being approximately 1.6 for reduced temperature at 2 °C below T_N. Optical textures were examined using a Carl-Zeiss Axio Imager.M1m polarizing microscope equipped with an AxioCam MRc5 digital camera. The sample cells (from M/s AWAT, Poland), were sandwich type, made of polyimide-coated, unidirectionally buffed ITO electrodes, providing uniform planar orientation of the nematic director $\mathbf{n}_o$; the cell gap d was 20 μm, unless otherwise stated. An Instec HCS402 hot stage coupled to a STC200 temperature controller maintained the temperature T to an accuracy of ±0.1 °C. A Stanford Research Systems function generator (DS345) connected to a FLC Electronics voltage amplifier (model A800) was employed for Fréedericksz reorientation. The field frequency f and rms voltage U were measured with a Keithley-2002 multimeter. We use a Cartesian reference system with the axes x and z along the rubbing and observation (or electric field) directions, respectively; $P(\alpha)$–$A(\beta)$ indicates the setting of the polarizer P and analyzer A with their axes at angles α and β (degrees) relative to x.

III. RESULTS AND DISCUSSION

A. N_{TB} drops in the isotropic environment

When a CB7CB-surfactant binary mixture, with a few wt % of the latter, is gradually cooled from the isotropic phase, we obtain, at first, the biphasic state consisting of nematic (N) droplets suspended in the isotropic (I) matrix. With continued cooling, N drops further nucleate, grow, and coalesce; subsequent transformations depend on the actual concentration of the surfactant. When it is low (as, e.g., in C-OP3), the entire sample eventually turns nematic prior to the onset of the N_{TB} phase, with the alignment governed by the cell type (planar or quarter-turn twisted); upon further cooling, we enter the second biphasic region comprising N_{TB} droplets in the N environment. As reported earlier [11], these drops occur as radial hedgehogs of +1 topological charge, rather than domains with focal conic defects; they are stabilized by the antidefects (hyperbolic hedgehogs or Saturn rings) that they create in their vicinity, in the surrounding nematic. By contrast, when the concentration of the surfactant is large (as, e.g., in COP7) the isotropic phase remains the dispersing medium in both the first and second biphasic states, in that, at the onset of the latter, the N_{TB} phase nucleates suddenly at numerous sites within each of the earlier N drops, even as new N_{TB} germs begin to appear in the isotropic matrix. This process is illustrated in Video V1, in the SM [16]. The N_{TB} drops are readily distinguished from N drops through their electric response; they remain stable against Fréedericksz reorientation at low voltages at which N droplets are discernibly perturbed. For example, the latter are detectably reoriented at 2 V in a high-frequency (10 kHz) field (at which ionic effects are negligible), while N_{TB} droplets are not affected even at 10 V.

We have previously reported the structural and electro-optic features of N drops in the isotropic environment [14]. Our main focus here is on the defect states of N_{TB} drops in the isotropic environment. Initially, N_{TB} droplets evolved directly in the I phase are structurally similar to those formed in the N phase. They appear as spherical objects exhibiting concentric birefringence color bands, as in Fig. 1(a). Further, as vividly seen in Fig. 1(b), the colors of the inner bands (region C) rise on the Newton scale with increasing radial distance r, while, at the boundary (region B) they fall. These optical path variations are expected [17] of drops that are hedgehogs, with a central +1 point. The corresponding pseudolayers

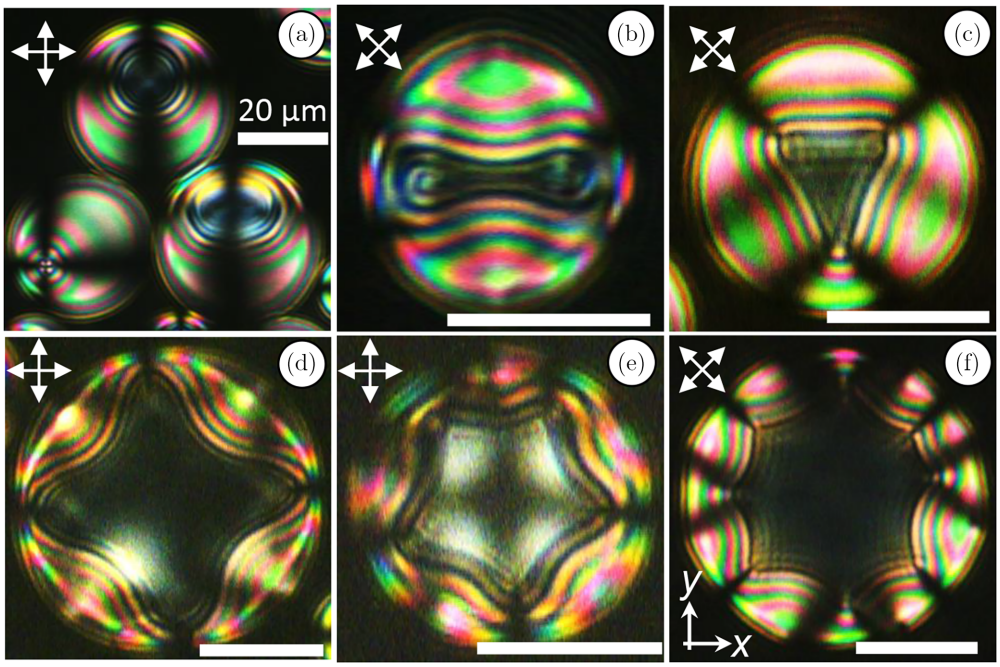

FIG. 3. N_{TB} drops in a 20 μm thick layer of C-OP5 in a planar cell. The point defects of the radial hedgehogs are enlarged into wavy loops of varying periods. No field is applied in (a); sine wave field of 10 kHz acts in (b–f); U = 12 V (b), 10 V (c), 15 V (d), 12 V (e), and 20 V (f).

of the N_{TB} phase, imagined as existing between successive planes of equivalent phase in the heliconical order, are concentric spheres [Fig. 2(a)]. This geometry corresponds to the anisotropy of surface tension, $\Delta\gamma = \gamma_{||} - \gamma_{\perp}$, being negative; here, the subscripts refer to the orientation of the pseudolayer normal relative to the interface normal. We may rule out the drops being toroidal focal conic domains (TFCDs), as the central order in such domains, schematically shown in Fig. 2(b), would show a decrease with increasing radial distance r, as illustrated in the inset to (b).

The purely splay type distortion that constitutes the radial hedgehog geometry of small N_{TB} drops does not sustain as the drop grows. This is revealed in two types of textural change. First, the drops become off centered with the point defect moving toward the boundary [Figs. 1(c) and 1(d)]. The $\boldsymbol{\chi}$ field would then involve both splay and bend, the latter being energetically more favorable [Fig. 2(c)]. Second, the extinction cross obtained with crossed polarizers, which is well defined in smaller drops [Fig. 1(a)], becomes progressively blurred at the center in larger drops of size exceeding the sample thickness; application of an electric field accelerates this realignment [Fig. 1(b)]. This general tendency of the central region to become homeotropic in flattened spherical drops is in agreement with $\Delta\gamma$ being negative; it involves the opening of the point defect into a disclination loop [Fig. 2(d)]. We may also expect deviation of the layer normal from surface normal when the anchoring energy is small and $\Delta\gamma$ is near zero (due to differing concentrations of the surfactant in the N_{TB} and I phases [18,19]).

The transformation of a point defect into a loop in a large flattened N_{TB} drop may be made to progress faster, as mentioned above, by the application of a high-frequency electric field E. While the loop into which a point defect expands spontaneously (i.e., in the absence of an electric field) is of circular outline, that formed under an applied electric field presents a wavy geometry. In Fig. 3 illustrating this effect, it is clear that the boundary of the drop develops many undulations under a strong electric field that dielectrically orients the $\boldsymbol{\chi}$ director of the drops along the layer normal all over, except the peripheral region. This instability at the edge finds a close analogy in a similar effect observed with smectic-A drops that nucleate in the electrically reoriented homeotropic nematic medium of a binary mixture of CB7CB and HOAB (4,4-diheptyloxyazoxybenzene) [20]. The growing drops, under a strong electric field, flatten into disks, with the smectic layers normal to the field $\mathbf{E}$ in their central region and periodically undulated at the boundary, with the edge distortion decaying exponentially inward; through its lens action, the distortion causes alternate dark and bright spots to appear in the optical texture, with the pattern period mainly determined by $\mathbf{E}$. The undulatory distortion is accounted for using the saddle-splay elasticity of the smectic phase that describes

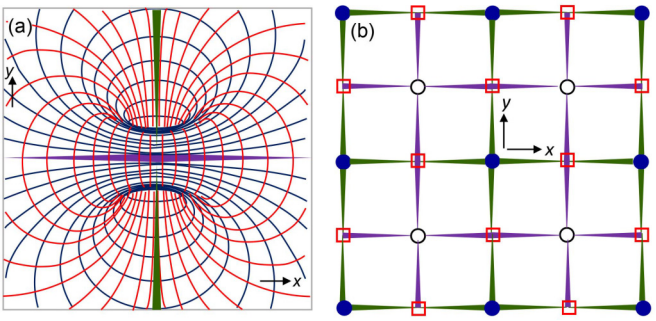

FIG. 4. Smecticlike behavior of the N_{TB} phase is reflected in its parabolic focal conic defect structure. In this state, the pseudolayers of the twist-bend nematic wrap around confocal parabolas (wedge-like lines in violet and bottle green) in orthogonal planes (a); a repetitive organization of defects appears along x and y at the top, bottom, and midregions of the N_{TB} slab (b). At the top, four parabolas meet at positions indicated by filled circles. A similar arrangement, indicated by open circles, exists at the bottom. The parabolas indicated by wedge lines cross over in the midregion at locations (in top view) indicated by squares. Notably, between crossed polarizers with their axes along x and y, dark extinction brushes are observed to run along x and y through the meeting and crossover sites of the parabolic lines.

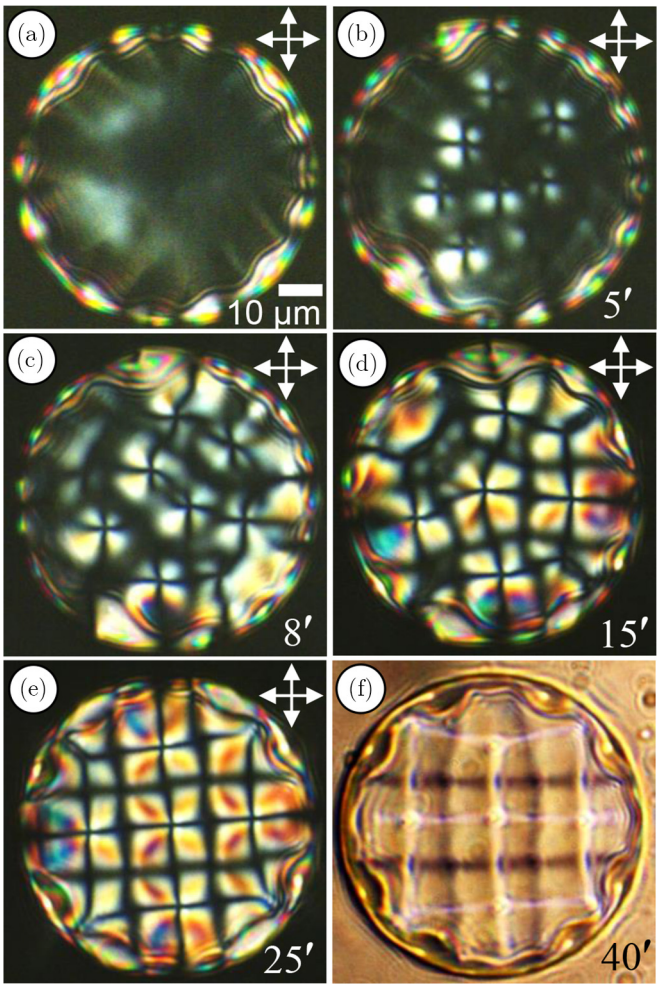

FIG. 5. (a) Texture at the start of a time series showing an N_{TB} drop subjected to a sine wave field (25 V, 10 kHz) rendering the drop homeotropic within its undulatory and birefringent circular boundary. (b–f) Select frames of the series after removal of the field showing gradual development of a PFCD network within the drop. Sample is a 5 μm thick layer of COP7 at 88 °C. Times indicated in minutes are relative to frame (a).

the Gaussian curvature of its layers [20,21]. Essentially, the negative saddle-splay contribution to the free energy is found sufficient to offset the positive contributions from the elastic splay and dielectric components of distortion. It seems, therefore, reasonable to think of the periodic edge distortion of the pseudolayers of N_{TB} disks as also stabilized by significant saddle-splay modulus k_{24}.

B. Evolution of PFCDs in N_{TB} drops in the isotropic environment

A common texture of the N_{TB} phase comprises parabolic focal conic domains (PFCDs). Generally, when this phase is derived from a uniformly planar extended N layer, one set of parabolas lies in the layer plane xy, while the other confocal set, in the orthogonal plane xz, with the axes of all parabolas along the rubbing direction x [7]. When the precursor N phase is homeotropically aligned along z, the confocal parabolas of the N_{TB} phase will organize into a regular network, with their axes along z [8]. The important structural features of PFCDs that manifest optically are described in the early reports by Rosenblatt *et al.* [22], and Asher and Pershan [23]. Some of them relevant to this study may be recalled with reference to Fig. 4. The geometry of Dupin cyclides associated with a pair of confocal parabolas is seen in Fig. 4(a). In an ideal array of such cyclides developed in an N_{TB} layer, the parabolas, which are the loci of cusps in the deformed layers, are organized repetitively, as in Fig. 4(b). The wedge lines represent the parabolic lines, their thin and thick ends terminating, respectively, at the bottom and top of the layer. At each of the repeating filled circles located on the assumed top surface, four parabolic lines meet, just as at the open circles on the bottom surface. The squares show the location of the crossings of parabolas in the midregion. The projection of the molecular director in the xy plane at each of the circles is radial; it is hyperbolic at the squares. Thus, when the PFCD texture is observed between crossed polarizers P(0)–A(90), the extinction crosses at the circles behave similarly to those of +1 disclinations; in other words, as the crossed polarizers are rotated, the brushes at the circles also rotate by the same angle and in the same sense. By contrast, the extinction brushes at the squares behave like those of –1 disclinations, rotating in a sense opposite to that of crossed polarizers. We may refer to these PFC defect sites as negative and positive sites.

In the background of the above description of the optical features of PFCDs, we may now consider the observed equilibrium textures of large N_{TB} drops, starting with the electrically excited state in Fig. 5(a). On switching the field off, the homeotropic central region of the N_{TB} drop, over a long period of time, will be filled with symmetrically organized PFCDs. Their progressive development is best seen in Video V2 (available in the SM [16]). Some select frames of this video are presented in Fig. 5. The texture in Fig. 5(f), which shows, in projection, the two sets of conjugate parabolas terminating at the two substrates in contrasting shades, is clearly representative of the schematic in Fig. 4(b).

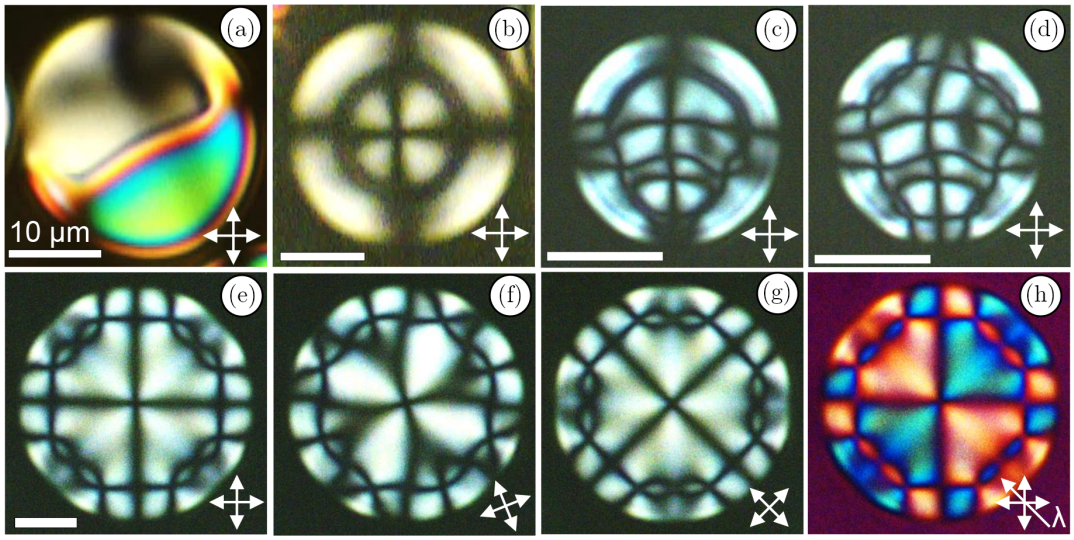

FIG. 6. Textures of an N_{TB} drop surrounded by the isotropic liquid of the same mixture, C-OP7, in a 5 μm thick layer, held in a 90 ° twist cell. (a) The drop at 89 °C, halfway through its transformation from being a radial hedgehog to a near-homeotropic, low-birefringence object. (b) Same drop as in (a), in the initial PFC state with a central +1 extinction site and a dark ring around it containing several developing PFC defects. (c–h) Further evolution of the PFC network, in a different drop similar to that in (a,b), on decreasing T through 0.2 °C from 88.6 °C. (c,d) Intermediate textures leading to the fully formed PFC network in frame (e) showing several symmetrically distributed extinction crosses, with the central cross being "positive" and adjacent crosses being of opposite sign; P(0)–A(90). (f) Rotation of the brushes with crossed polarizers revealing their sign; P(15)–A(105); (g) Appearance for diagonally crossed polarizers. (h) Upon insertion of a λ plate (with its slow direction across the indicated arrow) the birefringence color at positive sites increases on the Newton scale in the 1–3 quadrants relative to the 2–4 quadrants; the color change is reversed at negative sites; these changes apply when the planes of the parabolic defects contain the axes of P and A.

Even without any electrical reorientation, the N_{TB} drops nucleating as radial hedgehogs, as they grow to a size of the order of d, attain the equilibrium PFCD state through a series of structural modifications. In Fig. 6(a) marking the first stage of this process, the birefringent hedgehog is halfway through its transformation into a low-birefringence, near-homeotropic object that facilitates further development of parabolic cyclides. In Fig. 6(b), the central extinction cross, appearing as though due to a +1 line disclination, is actually a part of the evolving PFCD structure; the dark band around it contains other elements of the PFC network requiring further evolution to be optically resolved. Subsequent structural changes, indicated in Figs. 6(c)–6(e) (referring to a different drop), are readily seen in Videos V3 and V4 (available in the SM [16]); in the equilibrium state indicated by the texture in Fig. 6(e), the positive and negative PFCD sites occur alternately so as to form a symmetrical pattern. Whether the location of an extinction cross corresponds to a positive or negative PFCD site is readily determined by either following its rotation with crossed polarizers [cf. Figs. 2(e) and 2(f)] or monitoring interference color changes upon insertion of a λ plate [Fig. 2(h)]. In the latter case, the color rises, on the Newton scale, along the slow axis of the plate at +1 sites and along the opposite diagonal at –1 sites; these color changes apply when the planes of the parabolic defects contain the transmission axes of P and A. Accordingly, in Fig. 6(h), the central site is positive where four parabolas meet at a substrate; the four nearest sites around it, along x and y, are negative.

The equilibrium PFCD patterns developed in different drops of either the same size or different sizes generally vary in terms of the number of defects and their distribution. The defect sites organize symmetrically in many different ways determined by the course of their evolution. However, given sufficient time for equilibration, the defects distribute symmetrically in most cases, their texture in planform showing at least a vertical mirror element. In some instances, where the alternate positioning of positive and negative sites comes into conflict, the resulting metastable structure takes a long time to reorganize and reach the equilibrium. These characteristics are exemplified in Fig. S1 (available in the SM [16]).

As we shall discuss in a subsequent report, N_{TB} drops may be induced to undergo a drift motion under a suitable applied field. In the course of this motion, several drops may chance to come together to form organized clusters. Such clusters remain stable even on removal of the field and are observed to be associated with PFCDs. They are found with N_{TB} drops in either isotropic or nematic environments. In Fig. 7 presenting some examples of these clusters, it is seen that the –1 sites are at the junctions of adjacent drops [see encircled sites in Figs. 7(c) and 7(f)]; also, the number of confocal defect pairs formed and the number of parabolas meeting at the central +1 site equal the number of drops in the cluster. Thus, the arrangement of PFCDs here deviates from the regular square arrays of defects depicted in Fig. 4(b). An interesting feature of a cluster is that it acts as a single drop, which is evident particularly in a 90 ° twist cell, in terms of its binding modes with other drops through disclination knots (see Fig. S2 in the SM [16]).

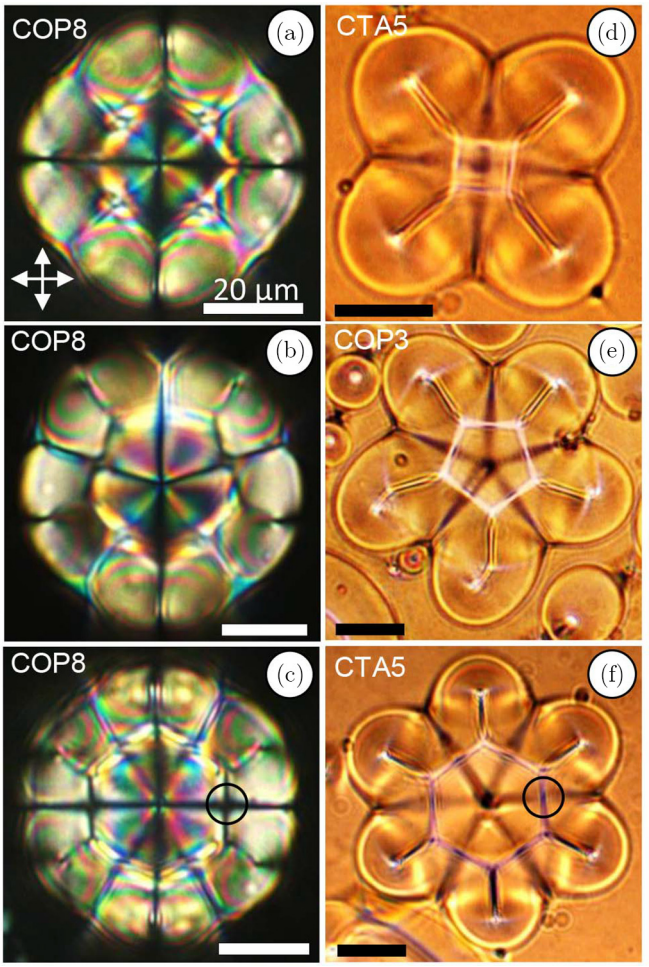

FIG. 7. Organized clusters of N_{TB} drops brought together under their electrically induced drift motion. These clusters remain stable after removal of the field. This association, involving PFCDs, is seen for the drops in either the isotropic (a–c) or nematic (d–f) environments; the sites such as the ones encircled in (c,f) are –1-like. The number of confocal defect pairs, and the parabolas meeting at the central +1 site, equal the number of drops in the cluster. Thus, the arrangement of PFCDs here deviates from the regular square defect arrays depicted in Fig. 4(b).

Well below the temperature of their nucleation, N_{TB} drops are large oblate spheroids containing many PFC defects; they appear as circular objects when viewed along their axes of symmetry. When heated from this state, the N_{TB} drops transform into nematic drops at about 1 °C above their onset temperature in the cooling run. Further, as their size and defect density diminish, the drops undergo a change of shape, with their boundary becoming angular. In particular, as exemplified in Fig. 8, the interface develops increased curvature near each of the peripheral defects. We may understand this as due to the surface tension anisotropy tending to vanish as the temperature increases. The angle between the normals of the pseudolayers and the interface is then not as much dependent on $\Delta\gamma$ as on the director field in the boundary region, which, in turn, involves the defects therein. Dependence of the shape of drops on changing $\Delta\gamma$ has

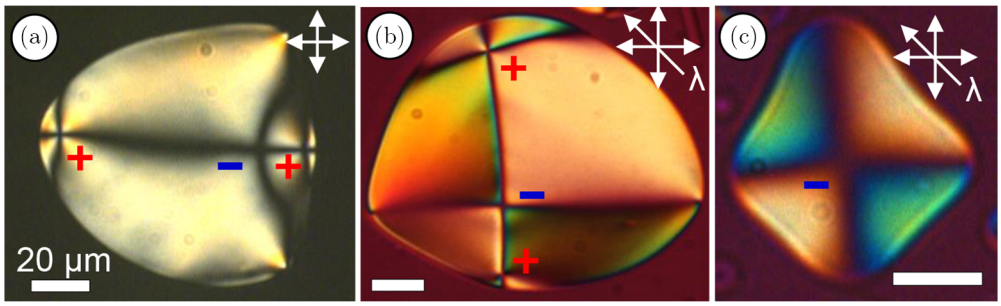

FIG. 8. N_{TB} drops of COP7 deviating from their circular planform geometry at higher temperatures. The drops in (a–c) are obtained by heating the drops of flattened spherical shape at 87.5 °C to 90 °C. The curvature of the boundary is noticeably increased near the peripheral defects.

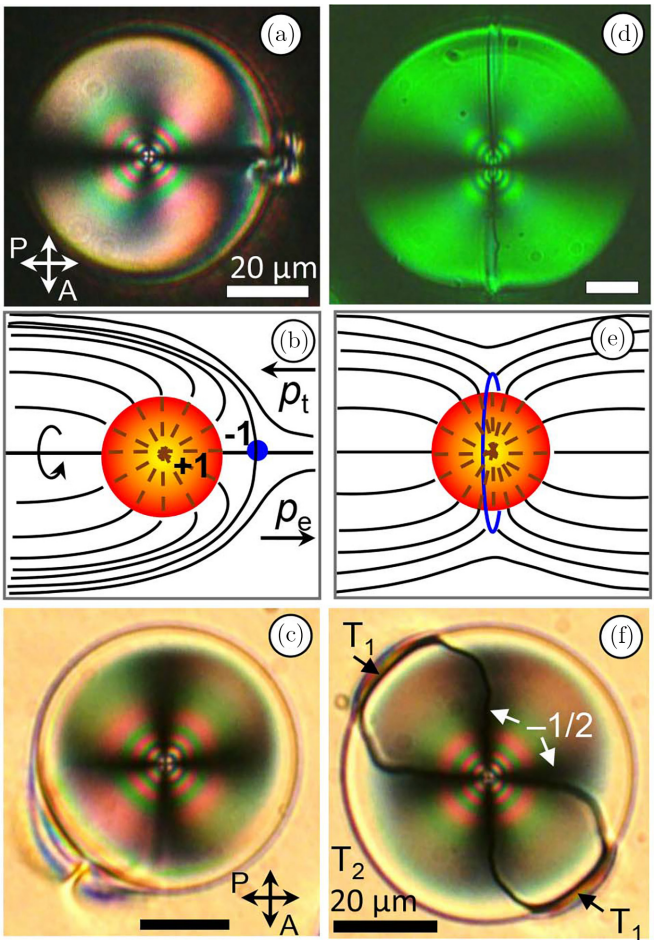

FIG. 9. N_{TB} drops acting as radial hedgehogs of charge +1 and creating in the host medium, close to the interface, counter defects to result in charge neutrality. Panels (a,c) show dipoles formed of radial and hyperbolic hedgehogs in planar and 90 ° twist cells, respectively; the dipole in (c) is along the midplane director $\mathbf{n}_M$. In panel (b) showing the director field corresponding to the dipolar geometry, p_t and p_e denote the topological and flexoelectric dipoles, respectively. Panels (d,f) show quadrupoles formed of N_{TB} drops and Saturn rings in planar and 90° twist cells, respectively; (d) is captured with a green filter. In (f), T_1 and T_2 indicate reverse twisted domains; wedge lines of strength –1/2 stretching along the substrate rubbing directions are bridged by twist lines so as to result in a figure of eight shaped unknot oriented along the normal to $\mathbf{n}_M$. Panel (e) shows the director field corresponding to the quadrupole in (d).

previously been discussed for smectic-*A* drops suspended in the isotropic liquid, in some binary mixtures of a smectogen and a surfactant [18,19].

C. N_{TB} drops in the *N* matrix: Transformation between point and ring disclinations

As previously reported [11], an N_{TB} drop in the radial hedgehog geometry attains stability either through its dipolar coupling with a satellite hyperbolic hedgehog [Figs. 9(a)–9(c)] or through its quadrupolar association with an equatorial Saturn ring [Figs. 9(d) and 9(f)], with the latter defects created in the enveloping nematic aligned unidirectionally in the far field. The relative stabilities of these topologically equivalent dipole and quadrupole geometries, in the absence of external fields, are known to be determined by elastic properties of the host medium, the diameter of the drop D, confinement ratio d/D (d being the sample thickness), and the anchoring strength W at the interface [24]. An early theoretical study of drops in inverse nematic emulsions using different variational ansatzes predicts dipoles as lower in energy compared to quadrupoles [25]. A later analysis [26,27] based on numerical minimization of the Frank free energy concludes micrometric particles with strong surface anchoring to be absolutely stable in the dipole geometry, and the Saturn-ring structure to be realizable on reducing the particle size or anchoring strength, as also on applying a magnetic field or using a nematic of large saddle-splay constant k_{24}. Similar results are also obtained in more recent theoretical-numerical studies based on the Landau–de Gennes Q-tensor free energy description [28–31]. Experimentally, micron-size water drops in a nematic matrix are indeed observed to form dipoles and dipolar chains [32–34]. However, calamitic nematic drops of similar size suspended in the matrix of a discotic nematic appear with the Saturn-ring geometry [35]; curiously, this experimental finding of 1990 marks the discovery of the Saturn ring preceding its theoretical prediction [36,37]. Quadrupolar geometry is also found with large ($D = 100$ μm) solid spherical particles dispersed in a thick ($d = 120$ μm) nematic layer [38]. This anomaly from the predicted behavior is attributed to the drops in strong confinement between the substrates as, in effect, acting as though they were subjected to a magnetic field [39].

In the light of foregoing results on the stabilities of dipole and quadrupole geometries, we now discuss our following findings:

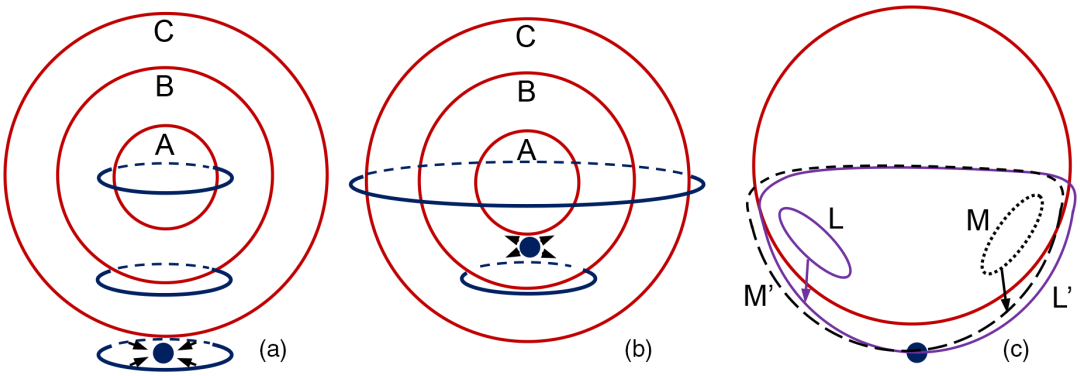

FIG. 10. Schematic of three scenarios of the quadrupole-dipole transition. (a) When a colloidal drop is small, it adopts the quadrupole configuration (A); as it enlarges, the ring drifts away from the equatorial position (B); when it is sufficiently large, the ring shrinks to a point (C). (b) When a colloidal drop is small, it adopts the dipole configuration (A); as it enlarges, the point defect opens into a loop (B); with its continued enlargement, the loop drifts progressively to the equilibrium position (C). (c) When the drop is large, over its hemispherical part carrying the point defect, a twist loop nucleates to relax the curvature strain; it develops into a D-shaped ring coupled to the point defect; the apparent linear segment of the D-like loop is a wedge type arc in the equatorial plane; in time, a second loop nucleates and enlarges into a D-like loop on the opposite side of the hemisphere; when the two loops meet at the point defect, the latter fuses completely and the two D arcs drift oppositely over the drop surface to form the Saturn ring.

(i) At its onset, the N_{TB} phase separates from the nematic as small spherical droplets coupled to the hyperbolic satellites they generate in the nematic. As the drops grow and become larger compared to d, the dipole structure becomes metastable and transition to the quadrupole geometry ensues in time.

(ii) Significantly, in the absence of any external perturbation, the dipole-quadrupole transition does not necessarily happen by the opening of a –1 point defect into a $-\frac{1}{2}$ ring, followed by a gradual drift of the latter with enlargement of the drop into the equilibrium, equatorial position [Figs. 10(a) and 10(b)]. The transition often begins with the nucleation of a loop disclination over the drop surface where the curvature strain in the nematic is large and this loop grows in time to entangle the hyperbolic defect. This metastable state may continue indefinitely.

(iii) The Saturn ring is completely formed when the loop enlarges further—the process hastened by an incremental decrease in T— and circumscribes the opposite hemispherical part. This final stage may involve nucleation and growth of a second loop disclination [Fig. 10(c)].

(iv) The radial hedgehog also develops into a ring in large N_{TB} drops. The geometry of this ring shows considerable variation, from triangular or circular when small to a starlike outline when large.

We present in Fig. 11 some select frames from a time series illustrating the course of transition of a dipole to a quadrupole in a nematic planar alignment cell (see Videos V5 and V6 in the SM [16]). In Fig. 11(a), a D-shaped loop is seen with its linear part along y in the equatorial plane and its curved part in contact with the hyperbolic hedgehog; while the linear part is finely focused, the curved part is increasingly defocused toward the satellite defect, indicating the loop as spread over a curved surface. This "midway" state of transformation remains unchanged for over 10 min, after which the temperature is marginally decreased. In a couple of minutes, a loop defect nucleates within the encircled part in Fig. 11(b) and it rapidly enlarges into a second D loop. From its overall defocused appearance as in Fig. 11(c), it seems to have formed over the opposite hemispheroidal part compared to the first loop. It is only when the two loops join at the –1 satellite defect that the latter disappears altogether. The curved parts of the D loops then drift oppositely over the hemispheroidal parts to form the Saturn ring in the equatorial plane. Figure 12 presents a similar sequence of changes marking the dipole to quadrupole transition in a 90 ° twist cell (see Video V7 in the SM [16]). In Fig. 12(a), we see the dipole along the midplane director and it is seemingly unaffected by the disclination D loop still in the process of enlarging. The quasistatic midway state of transformation again continues until the temperature is slightly reduced. A second D loop develops as a result, with the linear sections of the two loops along orthogonal directions corresponding to the alignment axes at the two substrates. The final Saturn ring wraps around the drop in a figure-of-eight unknot. It is to be noted that the $-\frac{1}{2}$ dark lines in Figs. 11(f) and 12(f) stretch fully across the drops, indicating the spheroidal drops as separated from the substrates by thin nematic films. The transformation just described is completely reversible, except for the hysteresis in regard to the drop size. The dipolar geometry is not realized until the N_{TB} drop shrinks, under increased T, to a size considerably smaller than it was at the dipole-quadrupole transition. After the transition to dipole, on decreasing the temperature marginally, the dipole begins to grow as in Figs. 13(f) and 14(h) and will not return to the quadrupole geometry before attaining a large size (Videos V8 and V9 in the SM [16] correspond to Figs. 13 and 14).

The intermediate state of dipole-quadrupole transformation, in which the hyperbolic hedgehog persists in contact with a D-shaped disclination, poses the important question of topological charge conservation. Assuming the loop as wedgelike in its straight segment and twistlike in the curved part, is it to be associated with a fractional ($\frac{1}{2}$) charge? Does the hyperbolic defect, then, carry a corresponding fractional

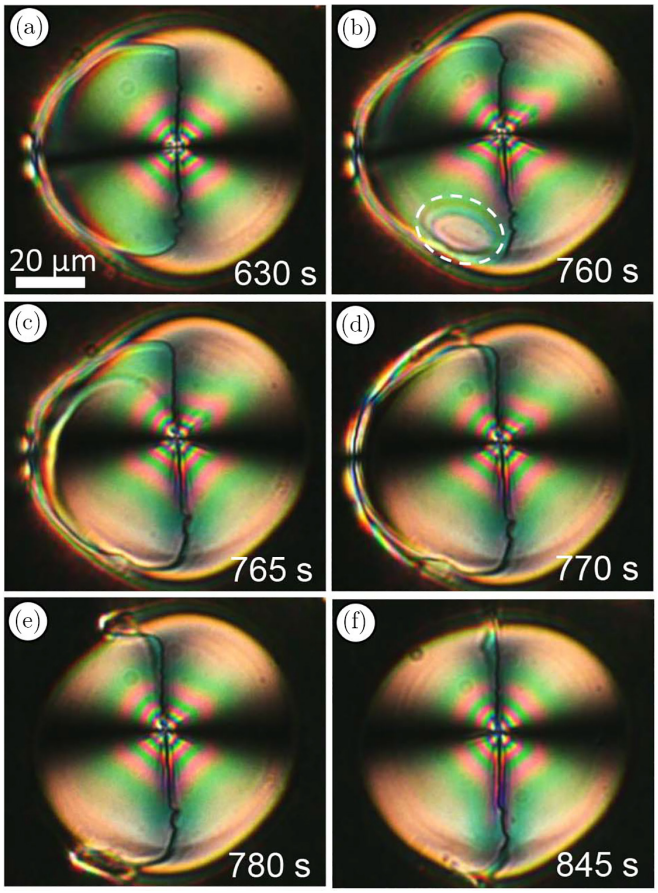

FIG. 11. The course of dipole-quadrupole transition in a 20 μm thick *C*-OP3 layer in a planar cell between crossed polarizers P(0)–A(90); $T = 92.2$ °C (a) and 92.1 °C (b–f). At 92.4 °C the texture was similar to that in (a), but the drop was smaller, measuring approximately 40 μm along *y*; the time series was started soon after decreasing T to 92.2 °C. Even at the end of 10 min, the transition remained partial as in (a). Then T was decreased by 0.1 °C. About 130 s later, a loop defect appeared within the encircled region in (b). When the enlarging new loop came in contact with the hyperbolic defect, the latter disappeared. The two D-shaped loops together formed the Saturn ring as in (f).

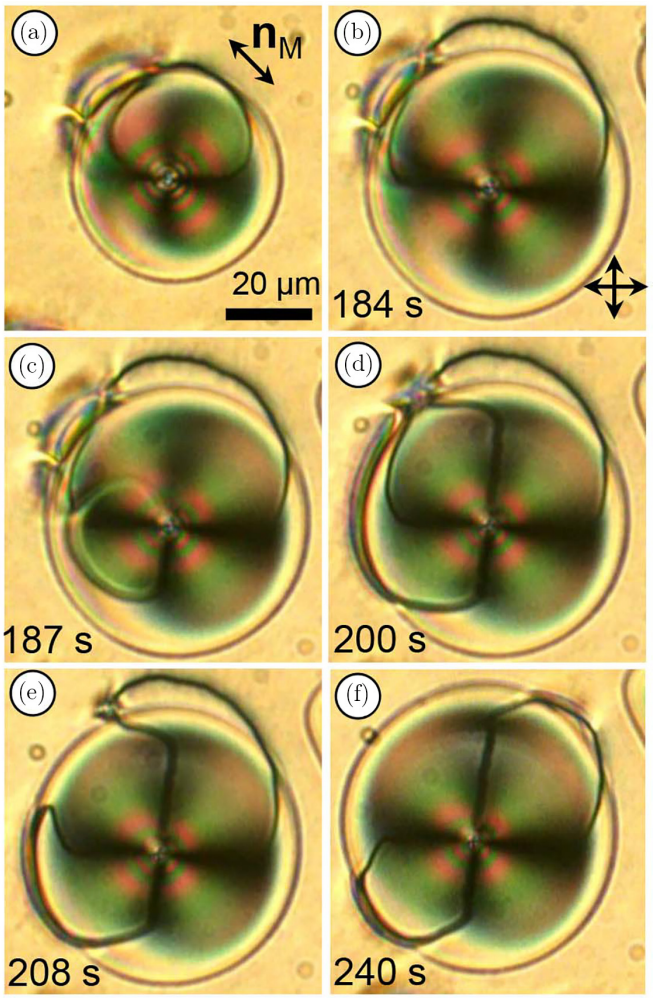

FIG. 12. The course of dipole-quadrupole transition in a 20 μm thick *C*-OP3 layer in a 90° twist cell between crossed polarizers P(0)–A(90). Starting with 92.3 °C in (a), T was decreased to 92.0 °C after 146 s. Subsequent textural changes at different indicated times are reproduced in (b–f). As may be seen, the transition was complete in about 4 min after the temperature drop. The state of partial ring formation in (a) remained unchanged until T was lowered.

charge? An alternative is to think of the D loop as only of twist type with no charge. Yet another option to preserve the charge invariance is to think of the –1 point disclination as having expanded into a tiny (optically unresolvable) loop of strength $-\frac{1}{2}$ that is in continuity with the D loop. Apart from the topological state of the point-ring hybrid geometry [Fig. 11(a)], there is also the question of the stability of dipole and quadrupole geometries with respect to drop size. Our results show some variance from earlier theoretical predictions mentioned at the beginning of this section. In fact, theories for spherical particles cannot be applied here when the drops are flattened spherulitelike objects or disks with rounded lateral boundaries. For example, if we consider the confinement ratio $\xi = D_z/(d–D_z)$, D_z being the vertical or z extension of the drops, it will have a large value for a drop sandwiched between thin separating nematic layers. Supposing ξ to be analogous to magnetic coherence length [39], we should expect the –1 point to open out into a loop of strength $-\frac{1}{2}$ going around the drop. However, dipolar geometry persists for drops with diameter D_x in the layer midplane far exceeding d. Additionally, as ξ decreases continuously—i.e., when a N_{TB} drop initially in the Saturn-ring geometry keeps shrinking under increasing temperature—the dipole geometry persists after the quadrupole to dipole transition, until the N_{TB} drop completely fuses (as seen in Videos V8 and V9 in the SM [16]).

Recently, Alama *et al.* [30] assessed energy minimizing configurations of the nematic director field around a spherical colloidal particle employing the Landau–de Gennes Q-tensor approach. They take the anchoring at the interface as weakly radial (homeotropic) and the undisturbed far-field alignment as uniformly planar. In the asymptotic regime of large particles, the Oseen-Frank energy minimizer is found to be the axisymmetric dipolar geometry; in the regime of small particles, the quadrupolar Saturn-ring geometry is found to be

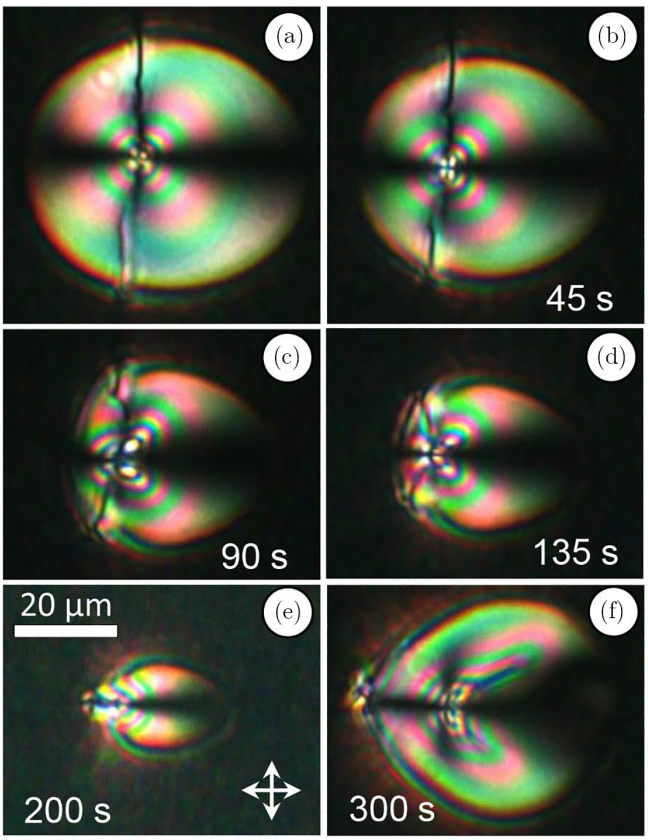

FIG. 13. Transformation of the Saturn ring around a N_{TB} drop into a hyperbolic hedgehog in an untwisted planar, 20 μm thick layer. $T = 89.3$ °C (a), 89.6 °C (b–d), 89.9 °C (e), and 89 °C (f). The N_{TB} drop is shrinking under increased temperature in (a–e); it is enlarging in (f) due to lowered T. Indicated times in (b–f) are relative to (a).

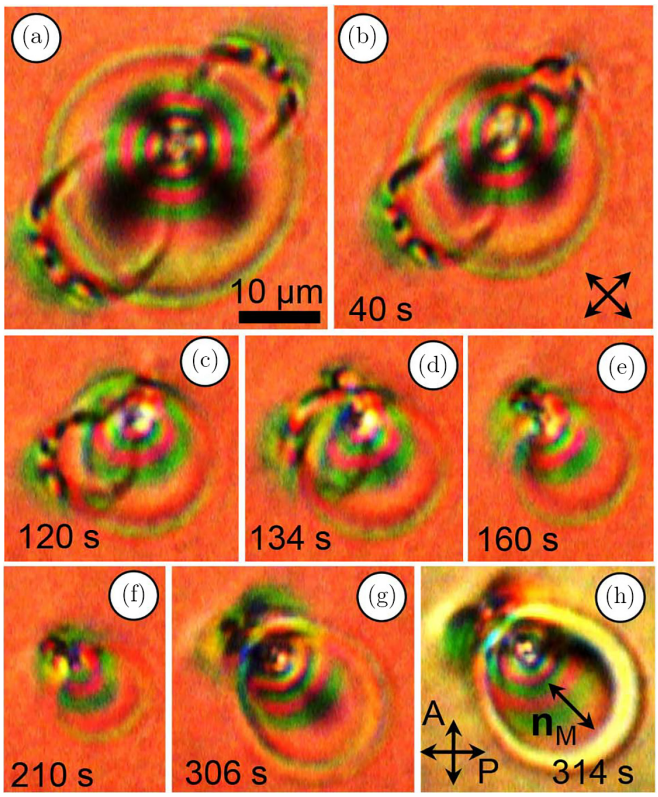

FIG. 14. Transformation of the Saturn ring around a N_{TB} drop into a hyperbolic hedgehog in a 90 ° twist cell of thickness 20 μm. The ring in (a) is an unknot, in the figure-of-eight geometry, oriented along the diagonal transverse to the midplane director $\mathbf{n}_M$; the dipoles in (e–h) lie along $\mathbf{n}_M$. In (a–f), the N_{TB} drop is shrinking under increased temperature (92.6 °C to 93 °C); in (g,h), the drop is enlarging at 92.8 °C. Indicated times in (b–h) are relative to (a).

favored. In a subsequent reassessment based on the same model, Alama *et al.* [31] demonstrate the possible existence of an equatorial Saturn ring around large particles even when the energy of this structure exceeds that of a smaller ring into which the hyperbolic point may expand close to the interface. This solution is conditional, occurring only in the limit of vanishing nematic correlation length.

D. Disclination knots in 90 ° twist cells

In a 90 ° twist cell, well below the N-N_{TB} transition temperature, the entire sample is divided into numerous oppositely twisted domains with all the N_{TB} drops dispersed in the nematic matrix bound up together by a common hybrid $\frac{1}{2}$ strength disclination composed of wedge and twist segments. The disclination forms a giant twisted knot that, in principle, can be completely unwound into a simple untwisted loop; hence it is topologically an unknot. We may recognize the giant unknot as being essentially constituted of three types of N_{TB} junctions. These are designated J1–J3 in Figs. 15(a)–15(c). Whereas, in J2 and J3, the Saturn-ring formation is complete, in J1 it is halfway through. A completed Saturn ring in the figure-of-eight geometry may open at one or both of the twist segments so as to bind with two or four neighboring drops. By contrast, the J1 bridges only two of its nearby drops. In Figs. 15(d)–15(h) showing different combinations of J1–J3, notably, a horizontal wedge line of one drop connects to the vertical line of another, implying that the twist line between the drops spans the sample thickness and appears, under diagonal polarizers, with periodic color bands (e). The steeper this oblique line the narrower are the bands (see Fig. S2 in the SM [16]); it is as though this line separates upper and lower regions of orthogonal optical axial directions, just as the diagonal plane in a Babinet compensator.

IV. CONCLUSIONS

In this study, we have examined the director geometries of twist-bend nematic drops formed in the matrix of nematic and isotropic phases, in binary mixtures of the mesogen CB7CB and a surfactant (2-octadecoxypropynol or tetradecanoic acid). The continuous phase in the biphasic state is nematic only for lower surfactant concentrations; it is isotropic for higher concentrations and this enables a study of the N_{TB} drops in the isotropic environment. While in both N-N_{TB} and I-N_{TB} biphasic states, the N_{TB} droplets form in the radial hedgehog geometry, their stabilities vary as they grow. In the N matrix, they retain the orthogonal boundary condition at the interface while growing; this stability is derived under topological neutrality, i.e., through formation of elastic dipoles or quadrupoles, in association with counterdefects

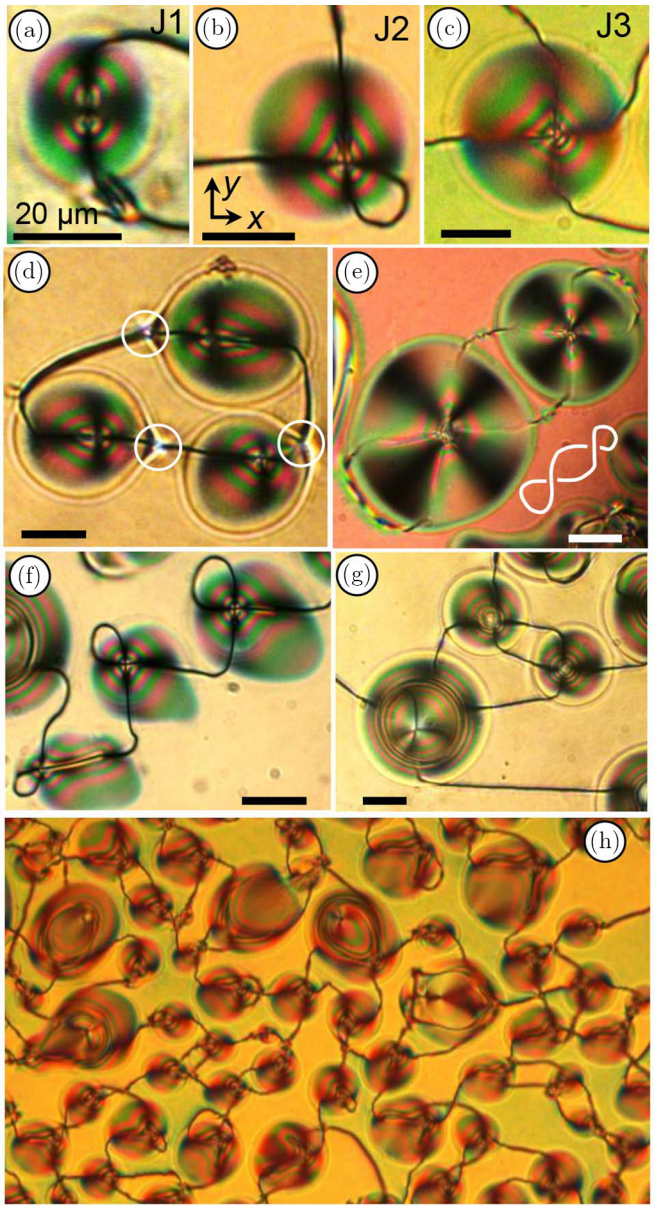

FIG. 15. (a–c) Three types of disclination junctions J1–J3 found at N_{TB} sites. The N_{TB} drops in (d) involve J1; in (e,f), J2; and in (g), J3. P(0)–A(90) in (a–d,f,g); P(45)–A(135) in (e). (h) A giant unknot involving all junction types; oppositely twisted regions here show a difference in color due to partial crossing of polarizers.

created in the nematic medium. By contrast, in the *I* matrix, centered radial N_{TB} drops, as they grow, first become escaped-radial-like, their director fields composed of both splay and bend. This birefringent metastable state transforms, in time, to a low-birefringence state in which the pseudolayers are largely in the sample plane, with slight distortions characteristic of the incipient PFCD state. Eventually, in the equilibrium state, the drops display networks of symmetrically disposed PFCDs. Turning to the *N* matrix, the dipoles and quadrupoles formed in it show several unique features not encountered in conventional nematic colloids with foreign particle dispersions. As a rule, smaller N_{TB} drops are very stable in the dipole geometry, and switch over to the Saturn-ring geometry only on growing to a size far exceeding the sample thickness. The transformation between the two geometries is reversible; a dipole obtained, under heating, from a shrinking quadrupole, as it becomes ever smaller while approaching fusion, persists with this geometry all through its existence. Notably, the dipole-quadrupole transformation often involves a metastable intermediate state in which neither the Saturn ring is completely formed nor the hyperbolic hedgehog completely fused. The topological state of this midway hybrid geometry remains an open question. In fact, the hybrid state features as a stable geometry in the formation of a complex unknot that binds all the N_{TB} drops formed in a 90 ° twist cell. Another noteworthy feature is the occurrence of dipole-quadrupole transformation mediated by nucleation of two new loop disclinations in the highly strained **n**-field region close to the interface, between the equatorial plane and the hyperbolic defect. Simulation of energy minimizer solutions that account for these unusual results relating to the stability of quadrupole and dipole geometries of very large spheroidal N_{TB} drops remains a challenging problem.

ACKNOWLEDGMENTS

The authors are thankful to Prof. B. L. V. Prasad for the experimental facilities, and to Prof. A. Jákli and Prof. I. I. Smalyukh for useful suggestions. C.V.Y. and D.S.S.R. acknowledge the financial support from the Science and Engineering Research Board (SERB), Department of Science and Technology [DST(IN)], Government of India, under Projects No. CRG/2020/001779 and No. CRG/2019/001671.

[1] M. Cestari, S. Diez-Berart, D. A. Dunmur, A. Ferrarini, M. R. de la Fuente, D. J. B. Jackson, D. O. Lopez, G. R. Luckhurst, M. A. Perez-Jubindo, R. M. Richardson, J. Salud, B. A. Timimi, and H. Zimmermann, Phys. Rev. E **84**, 031704 (2011).

[2] V. P. Panov, M. Nagaraj, J. K. Vij, Y. P. Panarin, A. Kohlmeier, M. G. Tamba, R. A. Lewis, and G. H. Mehl, Phys. Rev. Lett. **105**, 167801 (2010).

[3] L. Longa and W. Tomczyk, J. Phys. Chem. C **124**, 22761 (1920).

[4] S. M. Shamid, S. Dhakal, and J. V. Selinger, Phys. Rev. E **87**, 052503 (2013).

[5] R. B. Meyer, Structural problems in liquid crystal physics, in *Molecular Fluids*, edited by R. Balian and G. Weill (Gordon and Breach, New York, 1976), pp. 273–373.

[6] P. K. Challa, V. Borshch, O. Parri, C. T. Imrie, S. N. Sprunt, J. T. Gleeson, O. D. Lavrentovich, and A. Jákli, Phys. Rev. E **89**, 060501(R) (2014).

[7] S. A. Pardaev, S. M. Shamid, M. G. Tamba, C. Welch, G. H. Mehl, J. T. Gleeson, D. W. Allender, J. V. Selinger, B. Ellman, A. Jákli, and S. Sprunt, Soft Matter **12**, 4472 (2016).

[8] K. S. Krishnamurthy, M. B. Kanakala, C. V. Yelamaggad, and M. Kleman, Soft Matter **14**, 5393 (2018).

[9] A. Jákli, Y. Nastishin, and O. D. Lavrentovich, Liq. Cryst. Rev. (2022), doi: 10.1080/21680396.2022.2086932.
[10] M. Kleman and K. S. Krishnamurthy, Phys. Rev. E **98**, 032705 (2018).
[11] K. S. Krishnamurthy, D. S. Shankar Rao, M. B. Kanakala, C. V. Yelamaggad, and M. Kleman, Soft Matter **16**, 7479 (2020).
[12] C. Robinson, J. C. Ward, and R. B. Beevers, Discuss. Faraday Soc. **25**, 29 (1958).
[13] K. S. Krishnamurthy, D. S. Shankar Rao, M. B. Kanakala, and C. V. Yelamaggad, Phys. Rev. E **103**, 042701 (2021).
[14] K. S. Krishnamurthy, D. S. Shankar Rao, S. Sharma, and C. V. Yelamaggad, Phys. Rev. E **105**, 024709 (2022).
[15] P. Oswald, G. Poy, and K. S. Krishnamurthy, Phys. Rev. E **106**, 024705 (2022).
[16] See Supplemental Material at http://link.aps.org/supplemental/10.1103/PhysRevE.107.034706 for video clips V1.avi–V9.avi, and SM.pdf for video clip details and phase-transition related notes.
[17] R. B. Meyer, Mol. Cryst. Liq. Cryst. **16**, 355 (1972).
[18] R. Pratibha and N. V. Madhusudana, J. Phys. II **2**, 383 (1992).
[19] R. Pratibha and N. V. Madhusudana, in *Spatio-Temporal Patterns*, edited by P. E. Cladis and P. Palffy-Muhoray (Addison-Wesley, Boston, 1995), pp. 171–182.
[20] K. S. Krishnamurthy, D. S. Shankar Rao, M. B. Kanakala, C. V. Yelamaggad, and N. V. Madhusudana, Phys. Rev. E **101**, 032704 (2020).
[21] M. Kleman and O. D. Lavrentovich, *Soft Matter Physics: An Introduction* (Springer, New York, 2003).
[22] Ch. S. Rosenblatt, R. Pindak, N. A. Clark, and R. B. Meyer, J. Phys. **38**, 1105 (1977).
[23] S. A. Asher and P. S. Pershan, J. Phys. (Paris) **40**, 161 (1979).
[24] I. Muševič, *Liquid Crystal Colloids* (Springer, Cham, Switzerland, 2017).
[25] T. C. Lubensky, D. Pettey, N. Currier, and H. Stark, Phys. Rev. E **57**, 610 (1998).
[26] H. Stark, Eur. Phys. J. B **10**, 311 (1999).
[27] H. Stark, Phys. Rep. **351**, 387 (2001).
[28] J. -I. Fukuda, M. Yoneya, and H. Yokoyama, Eur. Phys. J. E **13**, 87 (2004).
[29] M. Ravnik and S. Zumer, Liq. Cryst. **36**, 1201 (2009).
[30] S. Alama, L. Bronsard, and X. Lamy, Arch. Ration. Mech. Anal. **222**, 427 (2016).
[31] S. Alama, L. Bronsard, D. Golovaty, and X. Lamy, Calculus Var. Partial Differ. Equations **60**, 225 (2021).
[32] P. Poulin, V. Cabuil, and D. A. Weitz, Phys. Rev. Lett. **79**, 4862 (1997).
[33] P. Poulin and D. A. Weitz, Phys. Rev. E **57**, 626 (1998).
[34] P. Poulin, H. Stark, T. C. Lubensky, and D. A. Weitz, Science **275**, 1770 (1997).
[35] R. Pratibha and N. V. Madhusudana, Mol. Cryst. Liq. Cryst. **178**, 167 (1990).
[36] E. M. Terentjev, Phys. Rev. E **51**, 1330 (1995).
[37] O. V. Kuksenok, R. W. Ruhwandl, S. V. Shiyanovskii, and E. M. Terentjev, Phys. Rev. E **54**, 5198 (1996).
[38] Y. Gu and N. L. Abbott, Phys. Rev. Lett. **85**, 4719 (2000).
[39] H. Stark, Phys. Rev. E **66**, 032701 (2002).